

CHAPTER - 4

Effect of dopants on Cadmium

Tungstate

4.1 Introduction

At present, there are very few reports available on rare-earth doped cadmium tungstate nanophosphors synthesized using hydrothermal method and study of their optical properties. An extensive spectroscopic study is required to completely understand the luminescent properties, including energy transfer mechanism and morphology of nano tungstates.

In this chapter, we present the rare earth (Ce, Nd, Eu and Er) doped CdWO₄ by low cost hydrothermal method around 100 °C temperature. The upconversion intrinsic luminescence has been observed for the first time in undoped as well as doped nano CdWO₄ powder samples when excited by 600 nm wavelength using xenon lamp. The effects of dopant on the crystallization, optical properties and size of particles were presented in this chapter.

In view of the literature survey, it is well known that nano sized inorganic low-dimensional systems exhibit a wide range of unique optical properties. Luminescent materials in the form of nanobelt, nanoparticles, nanorods, nanowires, nanotubes are of interest not only for basic research, but also for fascinating applications [1-2]. Divalent metal ion tungstates are of interest for their luminescent properties[3] and metal tungstate have good application prospects in scintillators, optical fibers, microwave applications, humidity sensors, photoluminescence materials, and catalysts, etc.[4-7]. Most of the tungstates have scheelite structure or wolframite mainly depending on their cationic radii. Small radii which are in favour of forming wolframite structure and large radii which are in favour scheelite structure

[8,9]. In wolframite structured tungstates the intrinsic luminescence is occurred from the annihilation of self - trapped excitation, and thereby forms excited $[\text{WO}_6]^{6-}$ complex that can be either excited in the absorption band or in the recombination process [10].

The tungstate doped with rare-earth nanophosphors have attracted special attention due to the corresponding bulk materials have large practical applications in solid state lighting and displays. It was also discovered that doping of cadmium tungstate (CdWO_4) with trivalent ions or monovalent ions is particularly effective in improving radiation sensitivity of the scintillator material [11]. Even rare-earth ions Ce^{3+} acts as common activators such that it will detect local environments due to their super-sensitive f-f transitions in some hosts [12]. Photoluminescence study of Ce^{3+} doped host materials have been studied widely, strong emission of Ce^{3+} is first observed in LaF_3 . In particular a host Ce^{3+} showed a very intense emission and in tungstates emission was quenched by Ce^{3+} doping [12]. Recently, M.You et al. demonstrated that $\text{CdWO}_4:\text{Eu}^{+3}$ is a promising red phosphor for blue based LEDs[13].

4.2 Rare Earth Elements

The rare earth (RE) ions most commonly used in applications as phosphors in laser materials for amplifier applications. They are also known as lanthanide ions. Luminescence of lanthanide ions has found numerous applications in medical diagnostics, optical fiber, night vision goggles, cathode ray tube (CRT), LED, sunglass lenses etc. The achievement in material science and nanotechnology of lanthanide luminescence has been using in cure of diseases. It is significantly used in drug delivery as a tracker of drugs delivered to infected cells [14-17]. The ground state of all the lanthanide atoms is probably either $[\text{Xe}] 4f^n 5d^1 6s^2$ or $[\text{Xe}] 4f^{n+1} 6s^2$, where the increase in n from 0 to 14 corresponds to the change from La ($Z=57$) through to Lu ($Z=71$). Rare earth ions have unfilled optically active 4f electrons screened by outer electronic filled shells. Because of these unfilled shells, these kinds of ion are usually called paramagnetic ions.

When lanthanide ions introduce in a host material, they effectively deactivated in organic host without any emission. On the other hand, inorganic hosts such as glasses and crystals have nominal non-radiative deactivation via excited lanthanide ions are observed. However, absorption band of lanthanide ions are weak in inorganic hosts. An efficient light absorption is obtained with incorporation of lanthanide ions in inorganic nanocrystals [17-19]. Therefore, selections of inorganic hosts which are nano crystalline in nature may be best suit the photoluminescence study of lanthanide ions doped materials. The structural and electronic properties are given in table 1.1.

Element	Z	A	Electron	Radius / pm		Crystal Structure	Lattice Parameters			
			Config	Ionic	Metallic		a / pm	c / pm	c / a	
Lanthanum	La	57	139	$4f^0 (5d6s)^3$	106.1	187.9	dhcp	377.4	1217.1	3.225
Cerium	Ce	58	140	$4f^1 (5d6s)^3$	103.4	182.5	fcc	516.1	—	—
Praseodymium	Pr	59	141	$4f^2 (5d6s)^3$	101.3	182.8	dhcp	367.2	1183.3	3.222
Neodymium	Nd	60	144	$4f^3 (5d6s)^3$	99.5	182.1	dhcp	365.8	1179.7	3.225
Promethium	Pm	61	145	$4f^4 (5d6s)^3$	97.9	181.1	dhcp	365	1165	3.19
Samarium	Sm	62	150	$4f^5 (5d6s)^3$	96.4	180.4	rhomb	362.9	2620.7	7.222
Europium	Eu	63	152	$4f^7 (5d6s)^2$	95.0	204.2	bcc	458.3	—	—
Gadolinium	Gd	64	157	$4f^7 (5d6s)^3$	93.8	180.1	hcp	363.4	578.1	1.591
Terbium	Tb	65	159	$4f^8 (5d6s)^3$	92.3	178.3	hcp	360.6	569.7	1.580
Dysprosium	Dy	66	163	$4f^9 (5d6s)^3$	80.8	177.4	hcp	359.2	565.0	1.573
Holmium	Ho	67	165	$4f^{10} (5d6s)^3$	89.4	176.6	hcp	357.8	561.8	1.570
Erbium	Er	68	167	$4f^{11} (5d6s)^3$	88.1	175.7	hcp	355.9	558.5	1.569
Thulium	Tm	69	169	$4f^{12} (5d6s)^3$	86.9	174.6	hcp	353.8	555.4	1.570
Ytterbium	Yb	70	173	$4f^{14} (5d6s)^2$	85.8	193.9	fcc	548.5	—	—
Lutetium	Lu	71	175	$4f^{14} (5d6s)^3$	84.8	173.5	hcp	350.5	554.9	1.583

Table 4.1 Structural and electronic properties (from Beaudry and Gschneidner 1978).

4.2.1 Crystalline field theory of rare earth ions

In crystalline field theory, the valence electrons belong to the RE ion and the effect of the lattice is considered through the electrostatic field created by the surrounding ligand ions at the RE position [20]. This electrostatic field is called the ‘crystal field’. It is supposed that the valence electrons are localised in RE ion and that the charge of the ligand ions does not penetrate into the region occupied by these valence electrons. The Hamiltonian can be written as [20] $H = H_{FI} + H_{CF}$. Where H_{FI} is the Hamiltonian related to the free ion (RE) which is an ideal situation in which the RE ions are isolated and H_{CF} is the crystal field Hamiltonian, which accounts for the interaction of the valence electrons of RE with the electrostatic crystal field created by the ligand ions. In order to apply quantum mechanical perturbation theory, the free ion term [20] is usually written as $H_{FI} = H_O + H_{ee} + H_{SO}$

Where H_O is the central field Hamiltonian which reflects the electric field acting on the valence electrons due to the nucleus and the inner- and outer-shell electrons, H_{ee} takes into account any perturbation due to the Coulomb interactions among the valence electrons, and H_{SO} represents the spin-orbit interaction summed over these electrons. Depending on the size of the crystal field term H_{CF} in comparison to these three free ion terms, different approaches can be considered of which the weak crystalline field approach describes the energy levels of the trivalent RE ions.

4.2.2 Weak crystalline field

$H_{CF} \leq H_{SO}, H_{ee}, H_O$. The energy levels of the free ion RE are only slightly perturbed (shifted and split) by the crystalline field [20,21]. The free ion wave-functions are then used as basis functions to apply perturbation theory, H_{CF} being the perturbation Hamiltonian over the $2^{S+1}L_J$ states. The shielding of the 4f valence electrons is considered to describe the energy levels of the RE ions using this approach. Consequently, the spin-orbit interaction term of the free ion Hamiltonian is dominant over the crystalline field Hamiltonian term. This causes the $2^{S+1}L_J$ states of the RE ions to be slightly perturbed when these ions are incorporated in crystals. The effect of the crystal field is to produce a slight shift in the energy of these states and to cause additional level splitting. However, the amount of this shift and the splitting energy are much smaller than the spin-orbit splitting, and thus, the optical spectra of RE^{3+} ions are fairly similar to those expected for free ions. Moreover, this implies that the main features of a RE^{3+} ion spectrum are similar from one crystal to another [20]. The free ion wave-function are then used as basis functions to apply perturbation theory, H_{CF} being the perturbation Hamiltonian over the $2^{S+1}L_J$ states (where S and L are the

spin and orbital angular momenta and $J = L + S$). This approach is generally applied to describe the energy levels of trivalent rare earth ions, since for these ions the 4f valence electrons are screened by the outer $5s^2 5p^6$ electrons. These electrons partially shield the crystalline field created by the B ions.

4.2.3 Cerium

The cerium atom ($Z=58$) has an outer electronic configuration $[\text{Xe}] 4f^1$ i.e. $5s^2 5p^6 5d^1 4f^1 6s^2$. Cerium is the most abundant member of the series of elements known as lanthanides or rare earths [22]. Cerium is the second and most reactive member of the lanthanides series. Cerium is characterized chemically by having two stable valence states one is Ce^{4+} , ceric, and the other is Ce^{3+} , cerous. It is very electro-positive and has predominantly ionic chemistry due to the low ionization potential for the removal of the three most weakly bound electrons. These atoms are usually incorporated in crystals as trivalent cations i.e. Ce^{3+} .

In lanthanide trivalent ions 5d, 6s, and some 4f electrons are removed and so $(\text{RE})^{3+}$ ions deal with transitions between electronic energy sublevels of the $4f^n$ electronic configuration. The $4f^n$ electrons are, in fact, the valence electrons that are responsible for the optical transitions. These valence electrons are shielded by the 5s and 5p outer electrons of the $5s^2 5p^6$ less energetic configurations. Because of this shielding effect, the valence electrons of Ce^{3+} ion are weakly affected by the ligand ions in CeWO_4 crystals; a situation results the case of a weak crystalline field. For Weak crystalline field: $H_{\text{CF}} \leq H_{\text{SO}}, H_{\text{ee}}, H_{\text{O}}$. Consequently, the spin-orbit interaction term of the free Ce^{3+} ion Hamiltonian is dominant over the crystalline field

Hamiltonian term. In this case, the energy levels of the free Ce^{3+} ion are only slightly perturbed (shifted and split) by the crystalline field.

4.2.4 Europium

The primary use of europium is in red phosphor in optical displays and television screens that use cathode-ray tubes and in fluorescent lamps [19]. It is also used in scintillators for X-ray tomography and as a source of blue color in light-emitting-diodes (LEDs) [17, 18, 23, 24]. In its predominant oxidation state of +3, europium behaves as a typical rare earth, forming a series of generally pale pink salts. The Eu^{3+} ion is paramagnetic because of the presence of unpaired electrons. Europium possesses the most easily produced and stablest +2 oxidation state of the rare earths [21].

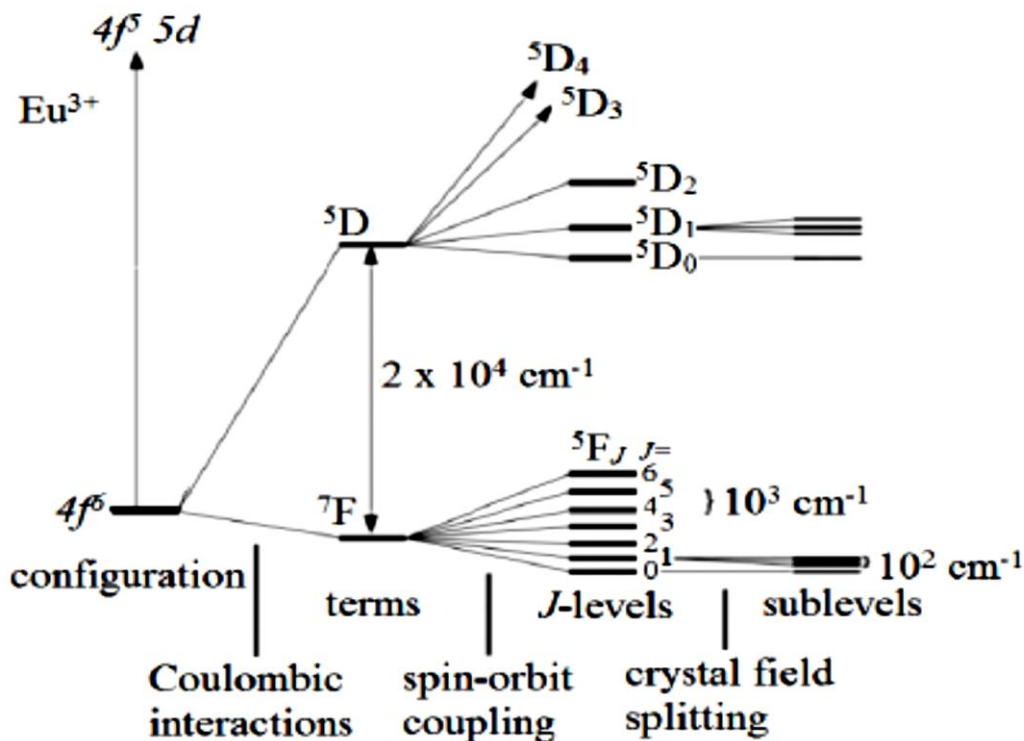


Figure 4.1 Electronic energy levels of Eu^{3+} ions

Europium is a lanthanide element and lanthanide ions are characterized by spectral peaks whose positions are independent of host matrix [19,20,27]. The Eu^{3+} peaks results from transitions within 4f shell which are shielded from surrounding by filled 5s, 5p and 6s shells, which are lower in energy, but spatially located outside the 4f orbital. Interactions leading to different electronic energy levels for the $[\text{Xe}] 4f^6 5d^0$ configuration of Eu^{3+} and hence the different peaks are shown in Figure 4.1. Coulombic interaction which represents the electron-electron repulsions within the 4f orbital is the largest interaction among the 4f electronic interactions. This interaction yield terms with a separation of the order of 10^4 cm^{-1} . These terms are split into several J-levels according to spin-orbit coupling with a separation of the order of 10^3 cm^{-1} . The individual J-levels are further split when the ion is presented in a coordinating environment such as a crystal which is referred to as crystal field splitting. The crystal field splitting is of the order of 10^2 cm^{-1} and it gathered information about the symmetry of the coordinating environment [17, 22, 24]. The main emissions of Eu^{3+} occur from $^5\text{D}_0$ to $^7\text{F}_J$ ($J = 0, 1, 2, 3, 4, 5, 6$) levels. The $^5\text{D}_0 \rightarrow ^7\text{F}_1$ transition is a pure magnetic dipole transition. This transition is practically independent of host matrix. The transitions from $^5\text{D}_0$ to the $^7\text{F}_J$ ($J = 2, 4, 6$) are pure electric dipole transition and they are strongly sensitive to symmetry of the host matrix. The remaining transition to $^7\text{F}_J$ ($J = 0, 3, 5$) levels are forbidden both in magnetic and electric dipole transitions and are usually found to be very weak in emission spectrum [19, 20, 25, 27].

4.3 Experimental Method

Cadmium Chloride ($\text{CdCl}_2 \cdot \text{H}_2\text{O}$), Sodium Tungstate ($\text{Na}_2\text{WO}_4 \cdot 2\text{H}_2\text{O}$) and Rare -earth Oxide were purchased from Alfa Aesar of analytical grade and used as received without any further purification. Distilled water was used as a solvent to prepare all required solutions. Initially 30ml solution of 0.1M concentration of $\text{CdCl}_2 \cdot \text{H}_2\text{O}$ was taken, subsequently another 30 ml solution of 0.1M concentration of $\text{Na}_2\text{WO}_4 \cdot 2\text{H}_2\text{O}$ was added into $\text{CdCl}_2 \cdot \text{H}_2\text{O}$ solution by dropwise and allowed for continuous stirring. To prepare sample, we added 30 ml solution of 0.01M concentration of Rare-earth Oxide (Ce, Nd, Eu and Er). These precursors solutions were transferred to Teflon-lined stainless-steel autoclave having 90 ml capacity filled with reaction media up to 80% one by one. The autoclave was maintained at a temperature around 100°C for 12 h and air cooled to room temperature. The prepared samples were washed several times with distilled water and lastly with absolute ethanol. Finally, a fine white powder was obtained after drying in vacuum at 80°C for 2 h. Figure 4.2 shows the flow chart to prepare the undoped and RE doped CdWO_4 using the hydrothermal method. The obtained phosphors are subjected to PL studies, XRD, FTIR and TEM. The characterization was done on the phosphors which emit highest PL intensity.

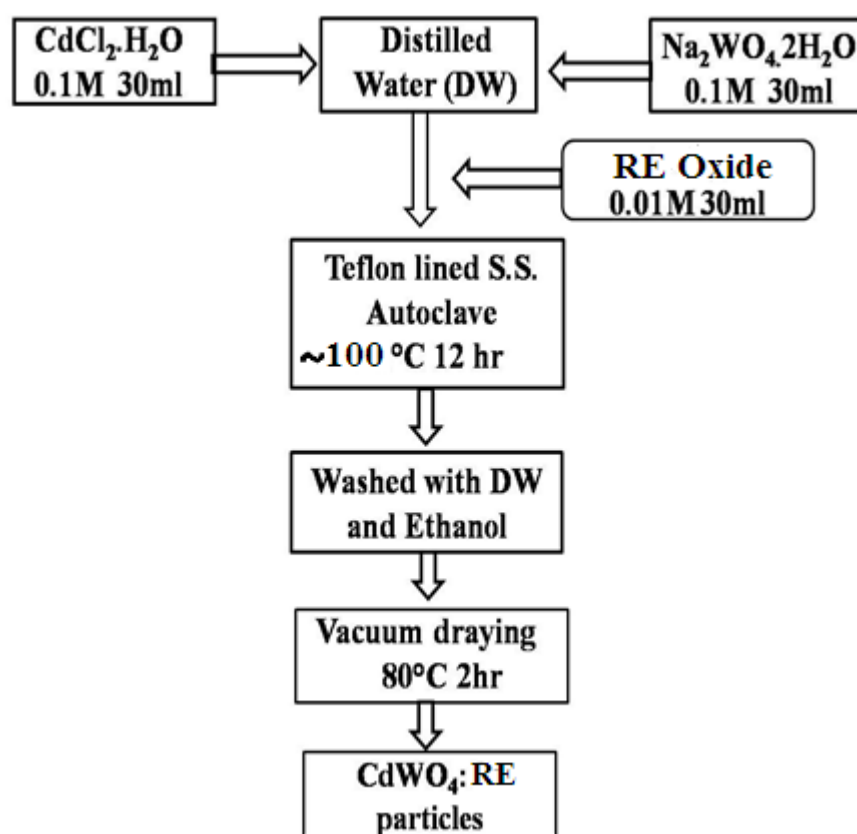


Figure 4.2 Flow chart of the synthesis process of CdWO₄ using the hydrothermal method.

4.4 Characterization

The XRD measurements were carried out with Japan Rigaku D/max X-ray diffractometer, using Ni-filtered Cu K α radiation. A scan rate of 0.05°/s was applied to record the patterns in the 2 θ range 10-70°. FTIR spectra recorded on a Jasco FTIR-4100, spectrophotometer (Japan) by mixing with KBr in mortar and pestle in the ratio of 1:10. The nanostructure and surface morphology of the CdWO₄ were observed by transmission electron microscopy (TEM, Tecnai 20 G2 FEI made). The PL of the samples was investigated on a Shimadzu spectrofluorophotometer at room temperature with a xenon lamp as excitation source.

4.5 XRD

From the figure 4.3, XRD patterns revealed that the CdWO₄ can be indexed to a pure monoclinic phase of CdWO₄ with a wolframite structure with space group P2/c (13) ; in agreement with JCPDS (Joint Committee on Powder Diffraction Standards) card No. 01-080-0139 and 01-080-0137.

Sample	JCPDS card No	Lattice parameters (Å)			Avg crystallite size(Å)
		a	b	c	
Undoped	01-080-0139	5.0110	5.8040	5.0500	15.31
Doped	01-080-0137	5.0280	5.8620	5.0670	14.70

Table 4.2 Lattice parameters and average crystallite size

The summary of lattice parameters and average crystallite size calculated using the Scherrer are given in table 4.2.

$$D = k\lambda/\beta\cos\theta$$

Where D is the average crystallite size, k is the constant equal to 0.89, λ is the wavelength of the X-rays equal to 0.1542 nm and β is FWHM.

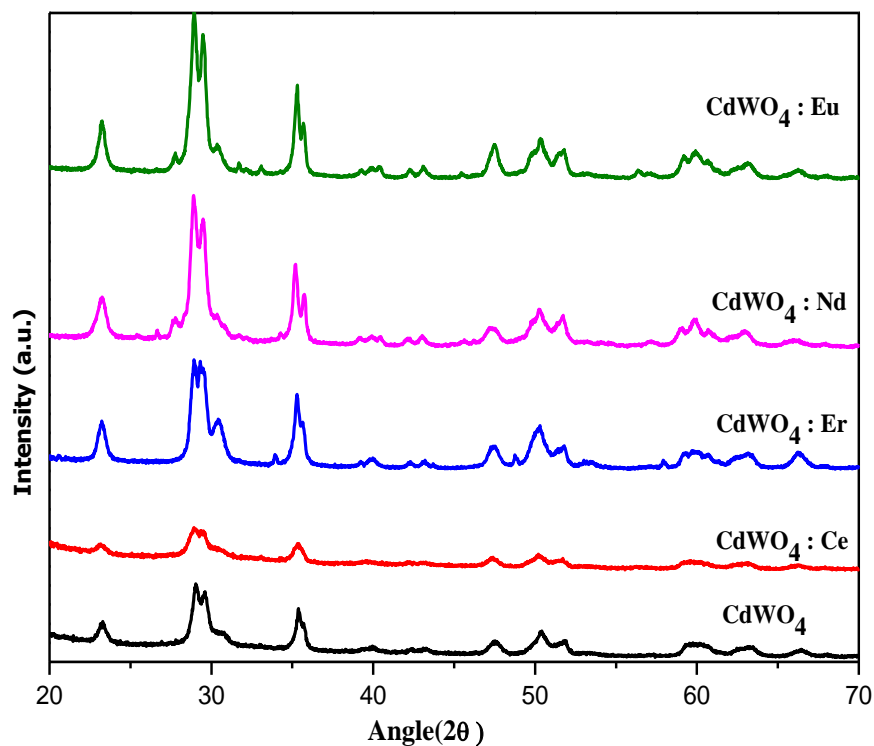


Figure 4.3 XRD patterns of undoped and RE-doped CdWO_4 (RE: Ce, Nd, Eu and Er)

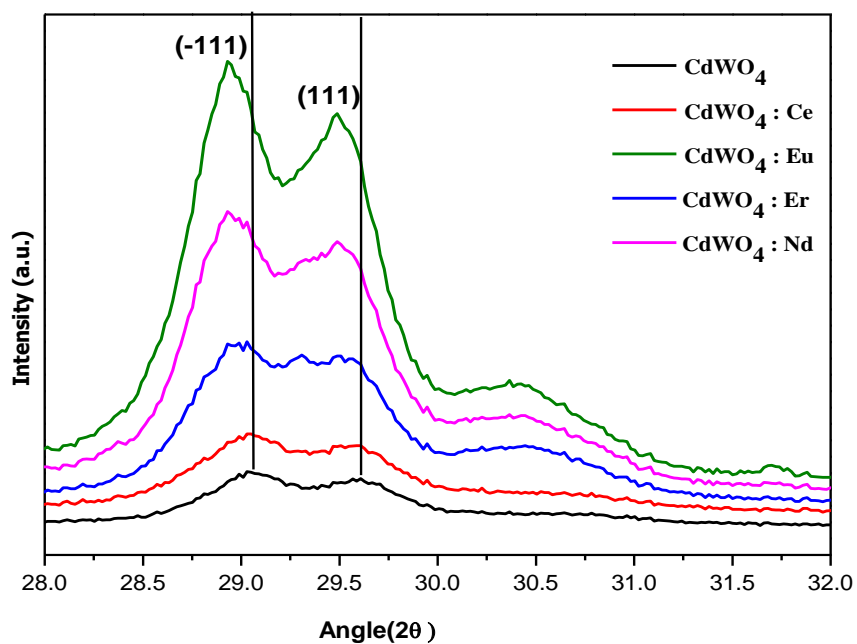


Figure 4.4 Comparison of the (-1 1 1) and (1 1 1) diffraction between of undoped and RE-doped CdWO_4 (RE: Ce, Nd, Eu and Er).

All the diffraction peaks in the patterns matched well with the standard data for cadmium tungstate (JCPDSNo. 01-080-0139, 01-080-0137) when the dopant (RE: Ce, Nd, Eu and Er) was doped in CdWO₄, no any other diffraction peaks belonging to the impurity phase were observed, which indicated that the products were purephase.

Figure 4.4 shows a careful comparison of the (-111) and (111) diffraction peak positions of CdWO₄: RE (RE: Ce, Nd, Eu and Er) in the range of angle 28° to 32°. It could be seen that the diffraction peaks of CdWO₄ shifted slightly to the lower angle when CdWO₄ is doped compare to undoped, which could be attributed to their placement of the Cd²⁺ by relatively larger RE³⁺.

According to Bragg's law,

$$d_{(h\ k\ l)} = \lambda / (2\sin\theta)$$

Where $d_{(h\ k\ l)}$ is the distance between crystal planes of (h k l), λ is the X-ray wavelength, and θ is the diffraction angle of the crystal plane (h k l) [26], the decrease in 2θ value should result from the increase in lattice parameters. Because the ionic radius of RE ion is larger than that of Cd ion, the observed shift of diffraction peak toward lower angles should be due to the larger lattice parameter expected for substitution of Cd²⁺ by RE³⁺. According to the XRD analysis, the dopants ions are incorporated into the lattice of CdWO₄, which clearly change the crystal field of the host lattice according to the chemical bonding theory of single crystal growth [27-29]. Therefore, the CdWO₄: RE (RE: Ce, Nd, Eu and Er) will exhibit different photoluminescence performances due to same concentration of different dopant.

Sr. No.	Phosphor	a(Å)	b(Å)	c(Å)	β	Volume(Å ³)	Crystallite size (nm)
1	CdWO ₄	5.05	5.84	5.08	92.50	149.70	16.50
2	CdWO ₄ :Ce	5.07	5.85	5.09	92.15	151.26	13.50
3	CdWO ₄ :Nd	5.054	5.882	5.08	92.25	151.08	10.23
4	CdWO ₄ :Eu	5.053	5.874	5.08	92.20	150.88	9.50
5	CdWO ₄ :Er	5.055	5.845	5.075	92.10	149.86	9.01

Table 4.3 XRD analysis of undoped and RE-doped CdWO₄ (RE: Ce, Nd, Eu and Er)

Table 4.3 is XRD studies of CdWO₄ and RE-doped CdWO₄ (RE: Ce, Nd, Eu and Er). Cell volume is calculated by computing cell parameters a, b and c from XRD data analysis. From the table 4.3, it is found that the volume of base CdWO₄ is 149.7 Å³. Similarly, the volumes of 0.005 M concentration RE (Ce, Nd, Eu and Er) doped CdWO₄ phosphors are also found. From this study, it is confirmed that when the atomic radius of rare earth dopant increases, the cell volume of corresponding rare earth doped phosphor decreases. The average crystallite size is also calculated from the XRD data and presented in table 4.3. The average crystallite size of CdWO₄ is 16.5nm. As the atomic radius of RE (Ce, Nd, Eu and Er) increases, the average crystallite size of corresponding RE (Ce, Nd, Eu and Er) doped CdWO₄ phosphors decreases. It is 13.5 nm for Cerium and 9.01nm for Erbium.

4.6 Photoluminescence (PL) Studies

Luminescence is a science, which closely related to spectroscopy in which substance emits light under the influence of certain incident radiation with the exception of pure heat. In 1852 English Physicist G.C.Stokes identified this phenomenon and expressed his law of luminescence now known as Stoke's law, which states that “the wavelength of the emitted light is greater than that of the exciting radiation.” German physicist E.Wiedemann introduced the term 'luminescence' (weak glow) into the literature in 1888. The phenomenon of certain kinds of substance emitting light on absorbing various energies without heat generation is called luminescence. Luminescence is obtained under variety of absorption and excitation process. The wavelength of emitted light exhibits characteristic and nature of the luminescent material. Substances emitting light are called luminophors or phosphors.

Light is incident on phosphors, where it is absorbed and imparts excess energy into the material in a process called photo-excitation. One way this additional energy can be dissipated by the phosphor is through the emission of light, or luminescence. In the case of photo-excitation, this luminescence is called photoluminescence. Photo-excitation causes electrons within a material to move into allowable excited states. When these electrons coming back to their equilibrium states, the surplus energy is released and may include the emission of light (a radiative process) or may not (a non-radiative process). The energy of the emitted light (photoluminescence) relates to the difference in energy levels between the two electron states involved in the transition between the excited state and the equilibrium state. The quantity of the emitted light is related to the relative contribution of the radiative process.

Photoluminescence spectroscopy is a contactless, non-destructive and highly sensitive method commonly used to study the photo-physical and photo-chemical properties in photo assisted reactions. It is closely related to the surface stoichiometry and the nature of surface states, which can usually be changed by the annealing process. Investigations have shown that the luminescence efficiency of materials can be improved by addition of appropriate impurity [11-13]. The PL emission is directly related to the recombination of excited electrons and holes, so the lower PL intensity indicates a delay in recombination rate and, thus, higher photo catalytic activity. In this section, the photoluminescence properties of doped and undoped CdWO_4 and comparative studies between different phosphor samples are also discussed.

4.6.1 PL Spectra of undoped and Ce doped CdWO_4

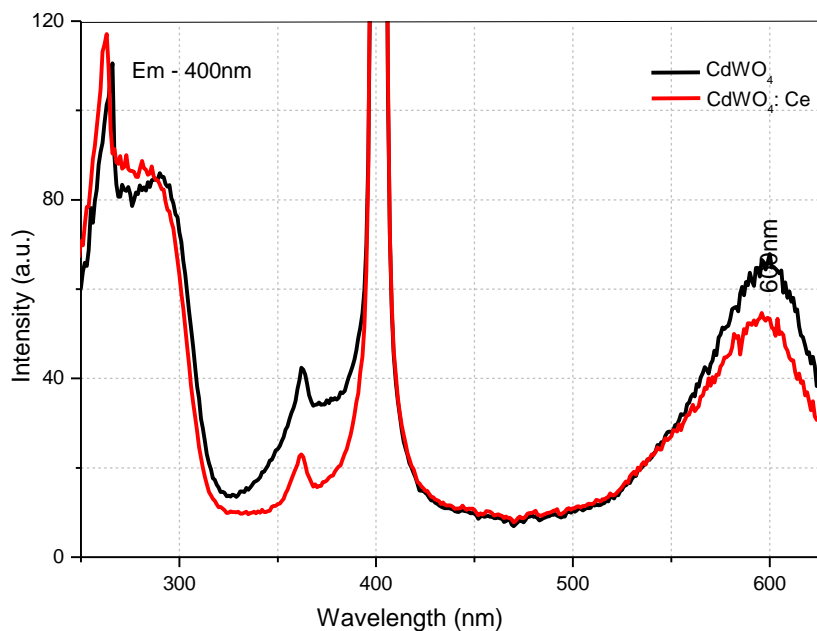


Figure 4.5 Excitation spectra of CdWO_4 and $\text{CdWO}_4:\text{Ce}$

The excitation spectra of undoped and Ce doped CdWO_4 phosphors recorded at Room temperature at 400nm emission wavelength is shown in figure 4.5. There is a broad absorption band between 220 nm and 325 nm, a small peak of very low intensity around 365nm and a broad peak centered around 600nm. The absorption intensity of the broad band centered around 600nm of undoped is greater than that of doped sample.

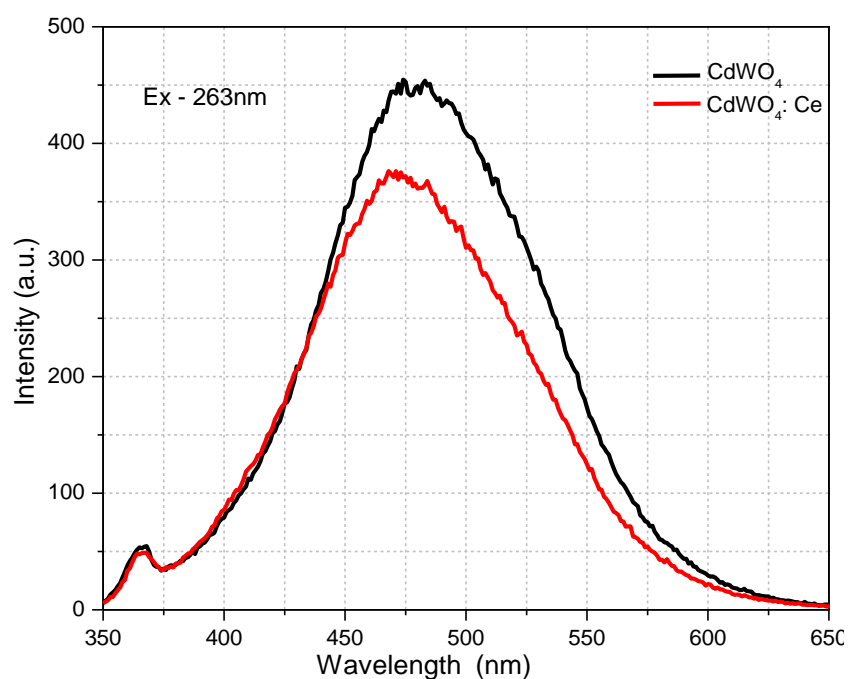


Figure 4.6 Emission spectra of CdWO_4 , $\text{CdWO}_4:\text{Ce}$ (Excitation wavelength: 263 nm).

Figure 4.6 and 4.7 exhibit PL spectra of undoped and cerium-doped CdWO_4 recorded at room temperature using 263 nm and 600 nm excitation wavelengths, respectively.

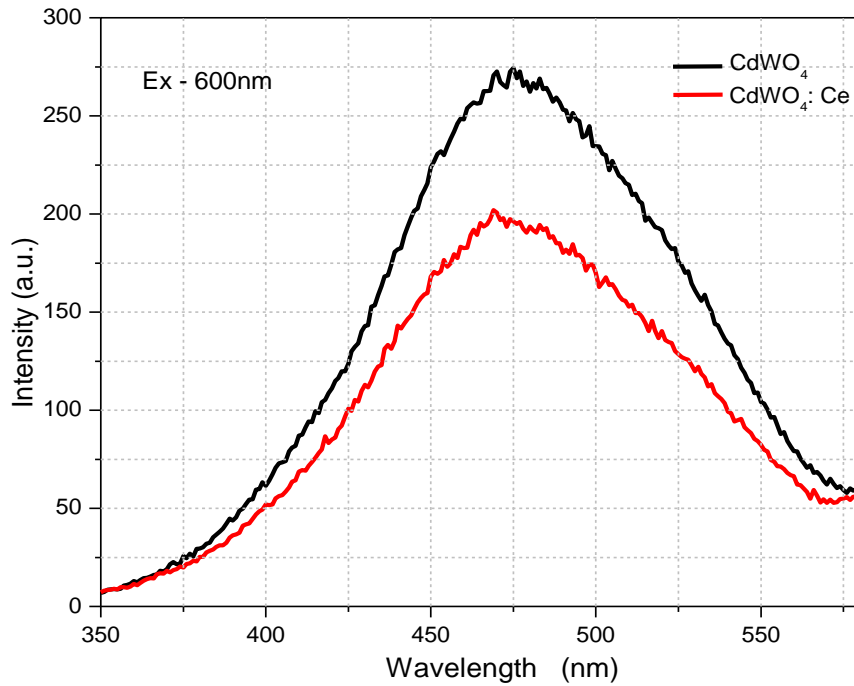


Figure 4.7 Emission spectra of CdWO₄, CdWO₄: Ce (Excitation wavelength: 600 nm).

From the figures, the photoluminescence spectra show broad intense peak at 474 nm and 475 nm wavelength in violet - green region peaking in blue region respectively. Interestingly, the luminescence intensity decreases when the cerium concentration increases in CdWO₄ as shown in figures 4.6 and 4.7. The luminescence observed in CdWO₄ is due to the intrinsic defects sites which are responsible and also due to self-trapped holes (STH) and radiative recombinations. As it is reported in the literature the PL emission with less intensity in mostly in blue region is due to WO₄²⁻. The presence of Cadmium with tungstate (WO₄) enhances 475 nm peak intensity and the emission spreads from violet to green region. Amount of energy 2.5 eV originating from the WO₄²⁻ group is mainly responsible for PL emission. It is stated in the

literature that the blue emission originates from the tetragonal WO_4^{2-} groups, while the origin of the green emission remains controversial [30].

The intensity of blue–green emission band is more at 263 nm excitation wavelength when compared with 600 nm excitation wavelength. It is due to higher stimulation energy of 263 nm (4.71 eV) excitation wavelength comparatively with 600 nm (2.06 eV) excitation wavelength. The cerium-doped sample shows weaker luminescence intensity than that of undoped sample in both the figures. The suppression of intensity is due to the nonradiative 5d–4f transition of the excited Ce ion. Therefore, Ce ions could serve as nonradiative traps in CdWO_4 crystal lattice [31]. The broad emission occurred between 425 nm and 525 nm may be obtained with the inclusions of the raspite structure formed due to the thermal stress appearing in the process of crystal growth [32-34]. It is well known that the luminescence spectrum of XWO_4 is composed of two main bands; the “blue” one peaking around 420 nm and the “green” one peaking between 490 to 540 nm. There are two defects: 1. regular lattice $(\text{WO}_4)^{2-}$ defect and 2. Defect based on WO_3 center, which are responsible for the complex character of CdWO_4 emission. The blue luminescence is an intrinsic feature of CdWO_4 , and is generally ascribed to the radiative decay of a self-trapped excitation that locates on the regular $(\text{WO}_4)^{2-}$ group [35]. The green luminescence is of extrinsic origin and it was ascribed to a defect based WO_3 center [36] possibly with F center [37]. PL spectra composed of several sub-bands which are almost distributed throughout entire 350-600 nm region. Such type of structural shape invokes presence of four to five Gaussian components. The presence of four-five Gaussian components indicates the excited states of emission centre are relaxed and degenerated under the influence of perturbation.

Excitation wavelength (nm)	Excitation energy (eV)	CdWO ₄			CdWO ₄ :Ce		
		Peak	Peak	Peak	Peak	Peak	Peak
		position (nm)	position (eV)	Intensity (a.u.)	position (nm)	position (eV)	Intensity (a.u.)
263	4.71	474	2.615	460	468	2.650	380
600	2.06	475	2.610	270	469	2.640	200

Table 4.4 Emission spectra analysis of CdWO₄ and CdWO₄: Ce.

From figure 4.7, the broad emission occurred between 425 nm and 525 nm when excited with 600 nm may be due to upconversion process occurred with reduced intensity at 475 nm of CdWO₄ and CdWO₄: Ce. The reason for reduction in intensity may be due to the increase of non-radiative transitions and or less excitation energy or with the increase in excitation wave length. The intensity of 475nm peak when excited with 600 nm is about 60 percentages of the PL emission intensity of 475nm peak when excited with 263nm. The excitation wave length, excitation energy, peak position, peak emission energy and peak intensity of CdWO₄ and CdWO₄: Ce are mentioned in table 4.4. When CdWO₄ excited to 263 nm varying the excitation energy is 4.71 eV, the emission is found at 475 nm. The average energy of 474 nm is 2.615 eV. When CdWO₄ excited at 600 nm whose electron energy is 2.06 eV, the average PL emission obtained at 475 nm varying electron energy 2.61 eV with intensity of 270 units. Similarly in Ce: CdWO₄ at 600nm (2.06 eV) excitation wavelength, the emission is found at 469 nm whose energy is 2.64 eV with 200 units intensity.

The similarity of PL spectra and possible observed up-conversion spectra for the nano CdWO₄ and CdWO₄: Ce phosphors suggest that emission centers may be same in both the cases. The up converted intrinsic luminescence emission exhibited by CdWO₄ and CdWO₄: Ce nanophosphors can be explained on the basis of anti-Stokes multi photon theory involving the capture of electrons in the intermediate levels due to d-d transition of Cd²⁺ ions. In both CdWO₄ and Ce: CdWO₄ phosphors, it is interesting to observe the possible up conversion; the up conversion process is as follow:

Upconversion process generally occurs due to two possible mechanisms (i) excited state absorption (ESA) and (ii) energy transfer upconversion (ETU) [38]. In the first mechanism a single ion is involved whereas two ions are involved in the second process [39]. In the ETU process the two excited ions which are present in intermediate state have a close affinity that are coupled by a nonradiative process in which one ion returns to the ground state while the other ion is promoted to the upper level. In most of the cases, these cross-relaxation processes are based on electric dipole - dipole interaction. In the present phosphors the Cd²⁺ ions absorb energy through d-d transition and transfer to WO₄ ions for intrinsic emission.

It is also observed from the figures 6 and 8 and table 4.4 that there is a minor peak shift of 6 nm which is mainly responsible due to the occupation of Ce³⁺ ions in the substitution positions of CdWO₄ host crystal lattice. From XRD and TEM measurements, it is inferred that both the samples will have same phase and structure. Therefore the shifting of peak does not relate with phase and it is attributed to doping of cerium. The position of the peak changes with the increase in

concentration of Ce^{3+} ions and shift in the wavelength occurred from blue to violet region [40].

4.6.2 PL Spectra of undoped and lanthanide (Ce, Er, Nd and Eu) doped CdWO_4

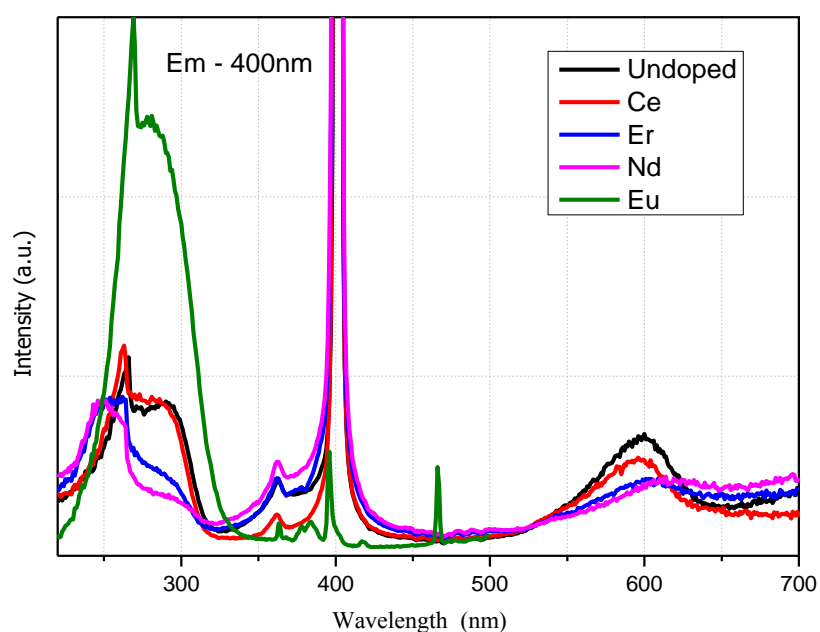


Figure 4.8 Excitation spectra of CdWO_4 and CdWO_4 : RE (RE: Ce, Nd, Eu and Er)

Figure 4.8 represents the excitation spectra of undoped and doped CdWO_4 . There is a broad absorption band between 220 nm and 325 nm, a small peak of very low intensity around 365 nm and a broad peak centered on 600 nm. The absorption intensity of the broad band centered on 600 nm of undoped is greater than that of doped sample. Excitation spectra of all samples have similar behaviour.

Figure 4.9 represents the emission spectra of undoped and doped CdWO_4 . PL spectra of undoped and doped CdWO_4 exhibit violet - green emission band peaking in blue region with a band edge UV emission. The intrinsic blue photoluminescence

originating from the tungstate group can be explained as follows: when the crystal is excited with above band gap energy, electron-hole pairs are created. The electrons are attracted only by W^{6+} ions because they are the most highly ionized and the holes will be attracted by O^{2-} ions. When electrons and holes recombine, the blue luminescence will occur. An electron from oxygen 2p goes into one of the empty tungsten 5d orbital (the bottom of W_{5d}) in the WO_4^{2-} group by absorbing ultraviolet irradiation in $CdWO_4$. In the excited state of the WO_4^{2-} group, the hole (on the oxygen) and the electron (on the tungsten) remain together as an exciton because of their solid interactions. This type of exciton which is produced in $CdWO_4$ is called Frenkel exciton where the radius of such exciton is very smaller. The exciton binding energy was estimated as being about 0.1 eV. The lowest exciton transition is connected to an electronic excitation from the mixed $Cd(5s) \rightarrow O(2p)$ ground states to the mixed $Cd(5s) \rightarrow W(5d)$ excited states. The Cd contributions to the top of the valence band and the bottom of the conduction band are small so the exciton transition is very weak. Such exciton is a molecular-type exciton of the WO_6^{6-} anion complex with covalent bonding within the Oxo-complex. The emission bands were attributed to the $^1A_1 \rightarrow ^3T_1$ transition within the WO_6^{6-} complex [41]. This is mainly due to the charge-transfer transitions between the O_{2p} orbital and the empty d orbital of the central W^{6+} of WO_6 octahedral or to the self-trapped exciton at a WO_6^{6-} oxyanion complex [42, 43]. The band edge UV emission may be due to recombination of free excitons through in exciton-exciton collision process or the radiative recombination of excitons bound to neutral donor [44, 45]. From the above result we can see that dopant do not affect the position of blue-green emission band in the 425 nm to 525 nm range. However, luminescence intensity of blue-green emission bands differs with different

dopant. Fluorescence emission originates from recombination of electron-holes. Low emission intensity intends that light-emitting material has a low recombination rate of electron-holes and a high separation rate of electron-holes at suitable excitation. In Cerium doped CdWO_4 the intensity of shoulder peak and main peak decreases when compared to undoped CdWO_4 which discussed in previous section. By comparing the intensity of characteristic peak of tungstate, mostly dopant which is added reduces the intensity.

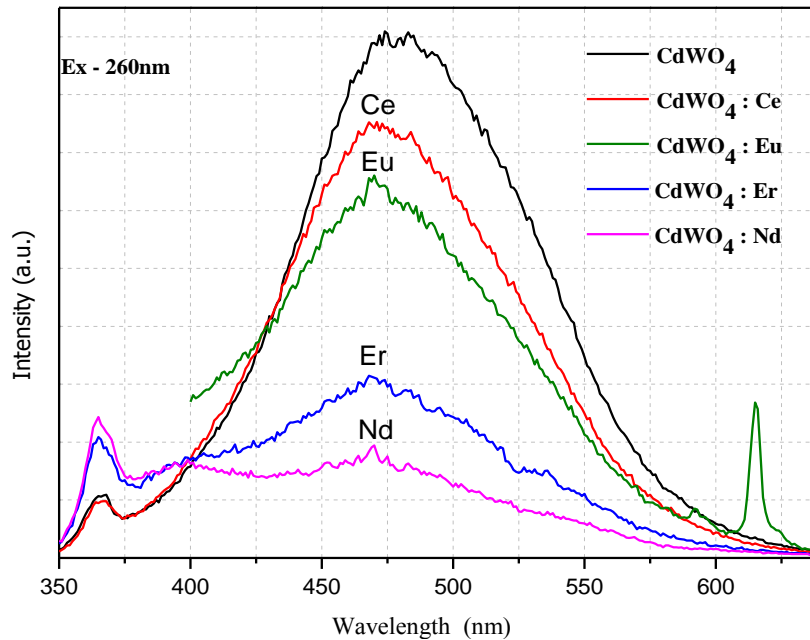


Figure 4.9 Emission spectra of CdWO_4 and CdWO_4 : RE (RE: Ce, Er, Nd and Eu)

The CdWO_4 : Eu phosphor has a blue-green emission peak at 470 nm in the PL emission spectra, with the excitation wavelength 260 nm as shown in figure 4.10.

For pure CdWO_4 sample, only one smooth peak centered at 470 nm was observed, which was due to the $^1\text{A}_1 \rightarrow ^3\text{T}_1$ transition within the WO_6^{6-} complex [41]. It is proposed that the WO_6 octahedral structure in CdWO_4 is the luminescent center. For CdWO_4 : Eu phosphor, not only typical emission of WO_4^{2-} but also yields the

characteristic emission of Eu^{3+} was observed and it contains the characteristic emission from the excited ${}^5\text{D}_0$ to ${}^7\text{F}_J$ ($J = 0$ to 3) of Eu^{3+} [46]. The peak at 613 nm is predominant out of all these peaks, this feature may be due to the ${}^5\text{D}_0$ - ${}^7\text{F}_2$ electric dipole transitions of Eu^{3+} . This phenomenon indicates that Eu^{3+} ions have been occupied the non-symmetry site in the CdWO_4 host lattice [47-49]. By doping the Europium, the PL intensity of CdWO_4 is decreased. This indicates energy transfer from WO_4^{2-} groups to Eu^{3+} and suggests effective doping of Eu^{3+} in the CdWO_4 lattice.

In Er doped CdWO_4 , different emissions are centered at 385nm, 405nm, 452nm, 476nm, 487nm, 518nm and 538nm are corresponding to the transitions ${}^4\text{G}_{11/2} \rightarrow {}^4\text{I}_{15/2}$, ${}^2\text{H}_{9/2} \rightarrow {}^4\text{I}_{15/2}$, ${}^4\text{F}_{5/2} \rightarrow {}^4\text{I}_{15/2}$, ${}^2\text{K}_{15/2} \rightarrow {}^4\text{I}_{13/2}$, ${}^4\text{F}_{7/2} \rightarrow {}^4\text{I}_{15/2}$, ${}^2\text{H}_{11/2} \rightarrow {}^4\text{I}_{15/2}$ and ${}^4\text{S}_{3/2} \rightarrow {}^4\text{I}_{15/2}$ respectively, were observed at room temperature [50-54]. With erbium concentration, the PL intensity of CdWO_4 is decreased. This indicates energy transfer from WO_4^{2-} groups to Er^{3+} and suggests effective doping of Er^{3+} in the CdWO_4 lattice. In CdWO_4 :Er the intensity of UV band edge is increased it may be due to more recombination of free excitons through in exciton-exciton collision process.

In Nd doped CdWO_4 , the characteristic peak of WO_4^{2-} group is weak intense compared to UV band edge peak. There is also one weak smooth peak observed and is centered at 400nm. This implies that transfer of energy occurred from WO_4^{2-} groups to Nd^{3+} which suggests successful doping of Nd^{3+} in the CdWO_4 lattice. Nd^{3+} is mainly responsible for enhancing the intensity in UV region. This indicates that Nd^{3+} is dominant in nature over WO_4^{2-} group.

From above study of different dopants in CdWO₄, it is inferred that Neodymium is highly effective and it offers highest energy transfer from WO₄²⁻ to Nd ions when compared to other dopant.

Sr. No.	Phosphor	Excitation wavelength (nm)	Excitation energy (eV)	Peak position (nm)	Peak emission energy(eV)	Peak Intensity (a.u.)
1	CdWO ₄			474	2.61	452
2	CdWO ₄ :Ce			468	2.65	376
3	CdWO ₄ :Nd	260	4.76	470	2.63	330
4	CdWO ₄ :Eu			469	2.64	156
5	CdWO ₄ :Er			470	2.63	97

Table 4.5 Emission spectra analysis of CdWO₄ and CdWO₄: RE (RE: Ce, Nd, Eu and Er)

The excitation wave length, excitation energy, peak position, peak emission energy and peak intensity of CdWO₄ and CdWO₄: RE (RE: Ce, Er, Nd and Eu) are mentioned in table 4.5. When the excitation energy 4.76 eV is applied to CdWO₄, the peak emission energy 2.61 eV is obtained with peak intensity 452 units. As dopant atomic radius increases from Cerium to Erbium, the PL intensity reduces. This may be due to more number of electrons present in Nd, Eu and Er leads to coulombic repulsion. Due to this repulsion the intensity gradually reduced by four times approximately i.e. for Cerium 376 units to Erbium 97 units.

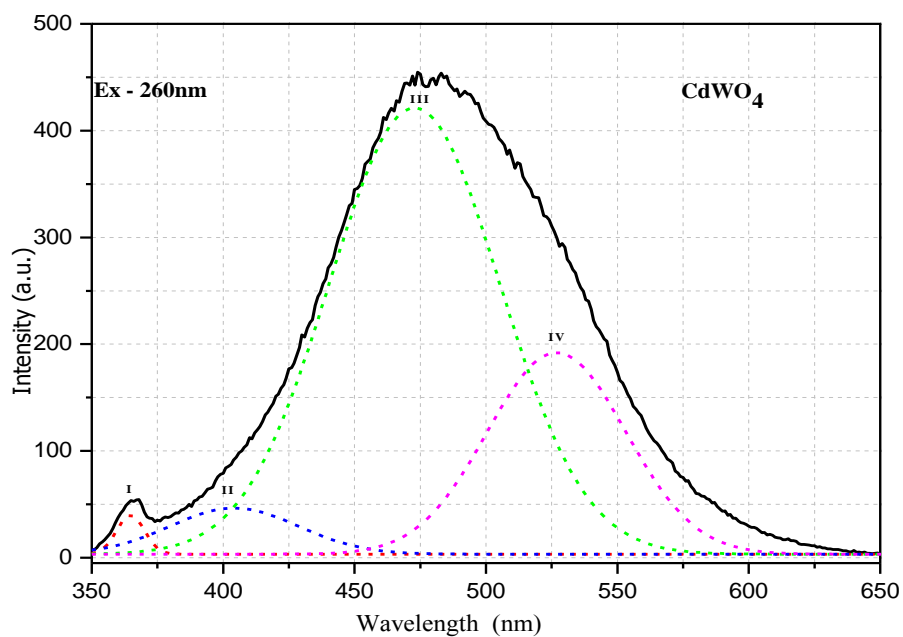


Figure 4.10a Gaussian peaks of CdWO₄

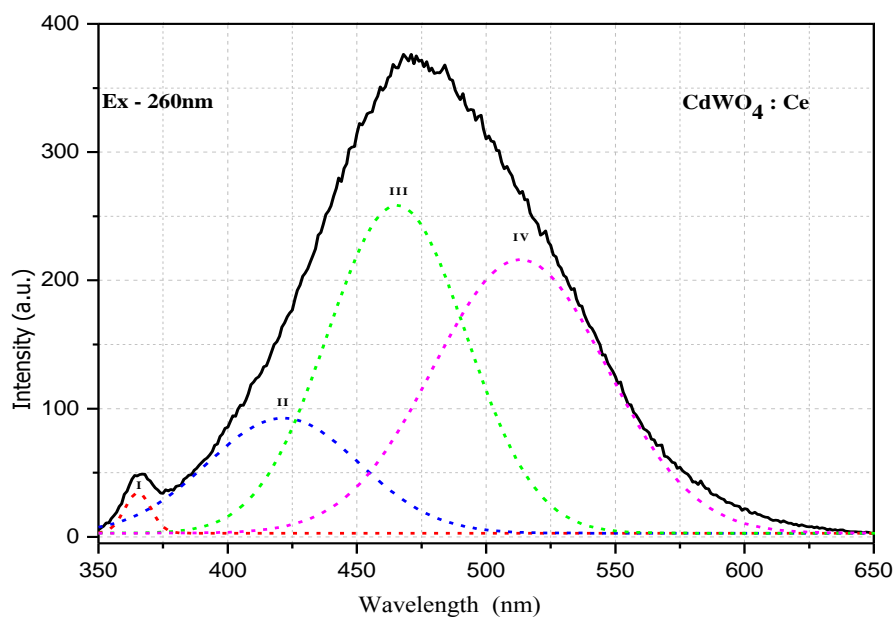


Figure 4.10b Gaussian peaks of CdWO₄:Ce

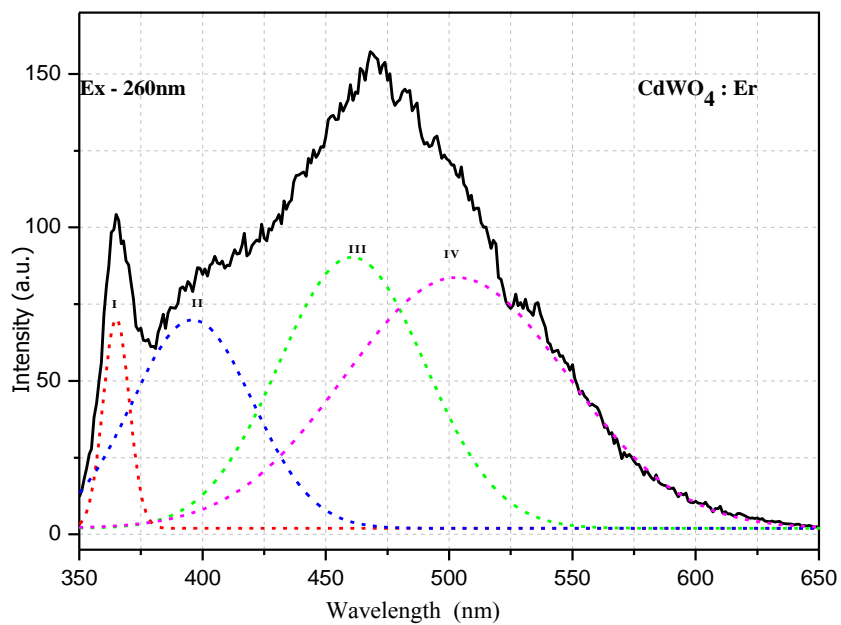


Figure 4.10c Gaussian peaks of CdWO₄: Er

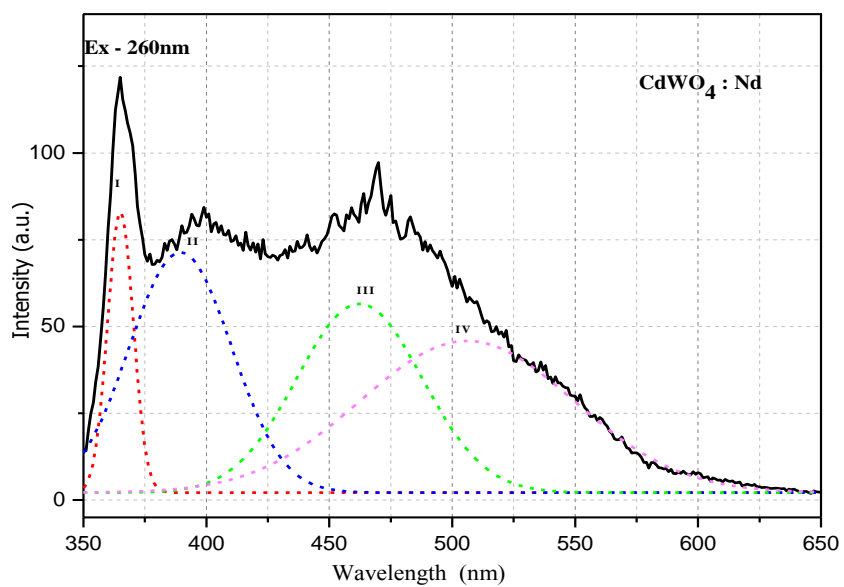


Figure 4.10d Gaussian peaks of CdWO₄:Nd

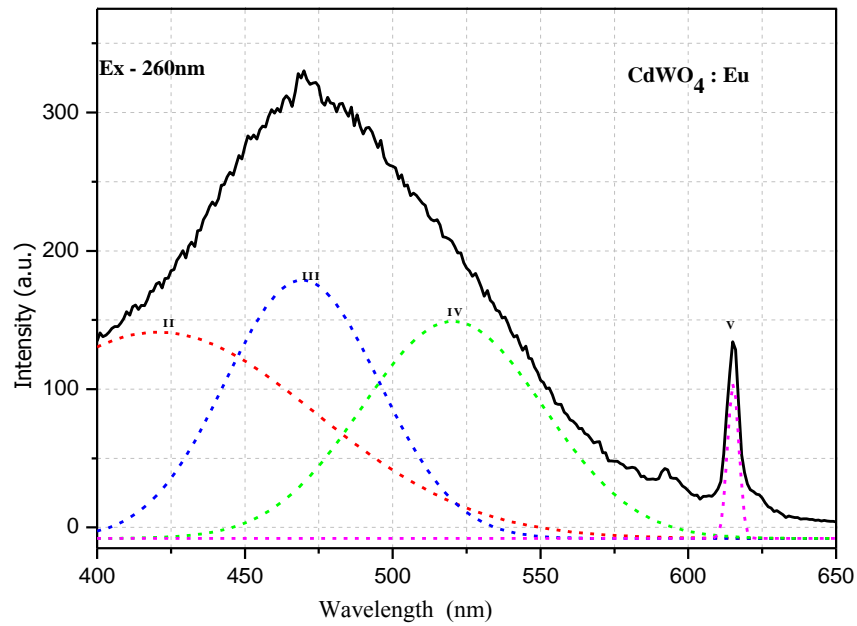


Figure 4.10e Gaussian peaks of CdWO₄:Eu

From the figure 4.10 (a to e), the Gaussian peaks of all samples are summarized in table 4.6. Here it is proposed that the Gaussian peak I (365 nm), the Gaussian peak II (392-422 nm) and the Gaussian peak III (458-473 nm) correspond to the radiative transitions of WO₄²⁻ and electronic transition of dopant in host matrix.

The Gaussian peak I observed in UV region and location is mentioned in a table 4.6. The G(I) band is dominant in Nd doped CdWO₄. The intensity of peak by Nd doped CdWO₄ has predominant nature than pure CdWO₄. Similarly in Er doped CdWO₄ significant increase intensity than the pure CdWO₄. This indicates that Nd and Er are effective dopants which play vital role in enhancing the emission in UV region of CdWO₄ host lattice.

The Gaussian peak II observed in violet region is mentioned in a table 4.6. The observed G(II) band is dominant in all doped sample. It indicates that Ce, Nd, Er and Eu are effective dopant which play vital role to enhance the emission in violet region in CdWO₄ host lattice.

Table 4.6 gives the information about the Gaussian peak III which is observed in 458 - 473 nm wavelength region. The G(III) band is dominant in undoped sample and it is the characteristic band of tungstate. This band is ascribed to the $^1A_1 \rightarrow ^3T_1$ transition within the WO₆⁶⁻ complex [37]. This is mainly due to the charge-transfer transitions between the O_{2p} orbital and the empty d orbital of the central W⁶⁺ of WO₆ octahedra or to the self-trapped exciton at a WO₆⁶⁻ oxyanion complex [15, 17]. In this region all dopant have reduced intensity in this band. The peak position of Gaussian components in PL spectra recorded at room temperature in all doped CdWO₄ is shifted towards the short wavelength side. Dopants are also responsible for small blue shift in this band. This type of blue shift is also reported by M.Itoh which was explained well by configurational coordinate diagram. Similar blue shift has also been observed in PbWO₄ [44] and CaWO₄ [45].

The Gaussian peak IV (505 - 527 nm) corresponds to green emission which is assumed to arise from oxygen deficient regular WO₃ group also called 'F' center. Oxygen vacancies VO (or F⁺⁺) can capture one or two electrons from [WO₄²⁻] to form 'F⁺' or 'F' centers and so [WO₄²⁻] is changed into WO₃. This emission as a result of the photo-thermally stimulated disintegration of localized exciton states and subsequent recombination of the produced electron and hole centres near WO₃ groups. This emission also ascribed to intrinsic luminescence probably originates from localized exciton in octahedral WO₆⁶⁻ groups in the wolframite phase.

Sample	Gaussian peak I		Gaussian peak II		Gaussian peak III		Gaussian peak IV	
	Intensity	Wavelength	Intensity	Wavelength	Intensity	Wavelength	Intensity	Wavelength
CdWO ₄	40	365	45	403	421	473	191	527
CdWO ₄ :Ce	34	365	92	421	258	458	216	516
CdWO ₄ :Er	70	365	70	398	90	462	84	505
CdWO ₄ :Nd	121	365	70	392	56	462	46	507
CdWO ₄ :Eu	-	-	-	-	179	469	148	521

Table 4.6 Position of Gaussian peaks of undoped and RE-doped CdWO₄ (RE: Ce, Er, Nd and Eu)

4.6.3 PL study of CdWO₄ doped with different concentrations of Ce.

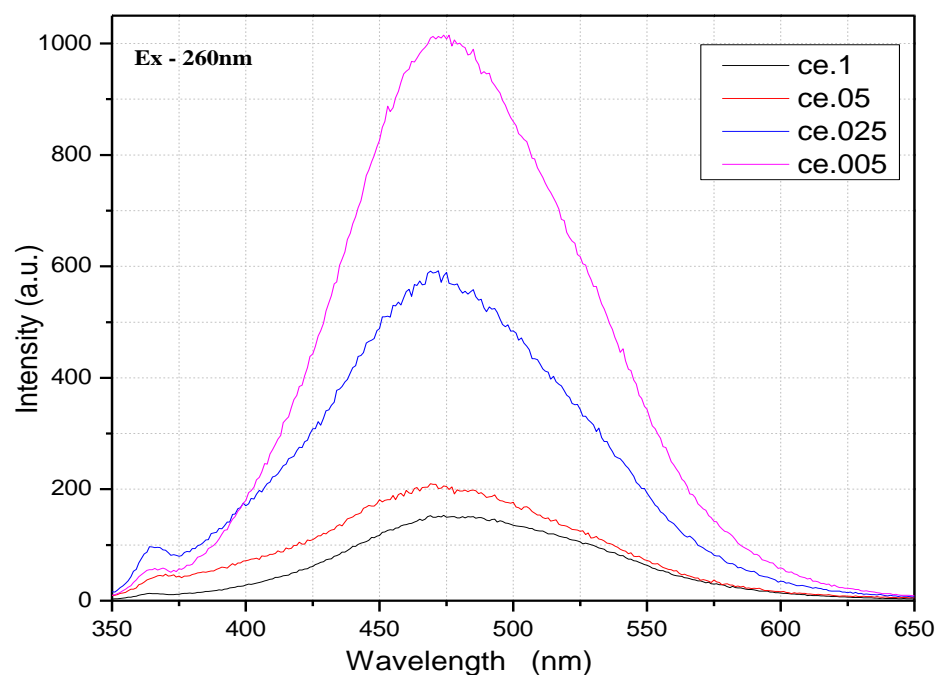


Figure 4.11 PL study of CdWO₄ doped with different concentrations of Ce.

Phosphor	Excitation wavelength (nm)	Excitation energy(eV)	Cerium Concentration (M)	Peak position (nm)	Peak position (eV)	Peak Intensity (a.u.)
CdWO ₄ :Ce	260	4.76862	.005	475	2.61	1008
			.025	469	2.64	587
			.05	469	2.64	210
			.1	470	2.63	152

Table 4.7 PL analysis of CdWO₄ doped with different concentrations of Ce

From figure 4.11 and table 4.7, it is observed that When CdWO₄ samples prepared with four different concentrations cerium it is observed that, by increasing the cerium concentration, the intensity of PL is reduced. This indicates that energy has been transferred from WO₄²⁻ groups to Ce³⁺ and it also suggests the effective doping concentration of Ce³⁺ in the CdWO₄ lattice. Due to higher concentration of cerium, the nonradiative 5d–4f transitions of the excited Ce³⁺ have been increased, which was observed in terms of suppression of PL intensity, is higher when compared to lesser concentration.

4.7 FTIR Studies

Figure 4.12 shows FTIR spectra at the wave number range of 400-4000 cm^{-1} of the CdWO_4 and Ce doped CdWO_4 . FTIR measurements were done using KBr method at room temperature.

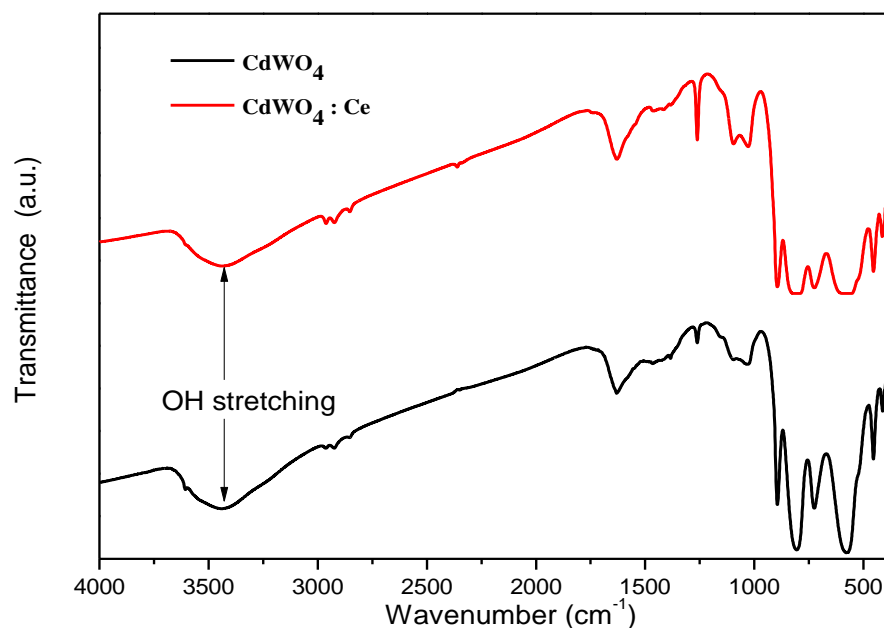


Figure 4.12 Room temperature FTIR spectra of CdWO_4 and $\text{CdWO}_4:\text{Ce}$

The bending and stretching vibrations of Cd-O (542cm^{-1}), W-O (681 cm^{-1}) and Cd-O-W (823 cm^{-1}) were observed in the undoped as well as doped CdWO_4 . The FTIR spectrum of sample b exhibits broad band below 700 cm^{-1} which is due to the δ (Ce - O-C) mode [55]. The absorption peaks exhibit bands around 1626 and 3448 cm^{-1} may be attributed to O-H stretching mode of water. Residual water - hydroxy groups may be due to absorption of water molecules from atmosphere [56].

4.8 Transmission Electron Microscopy (TEM)

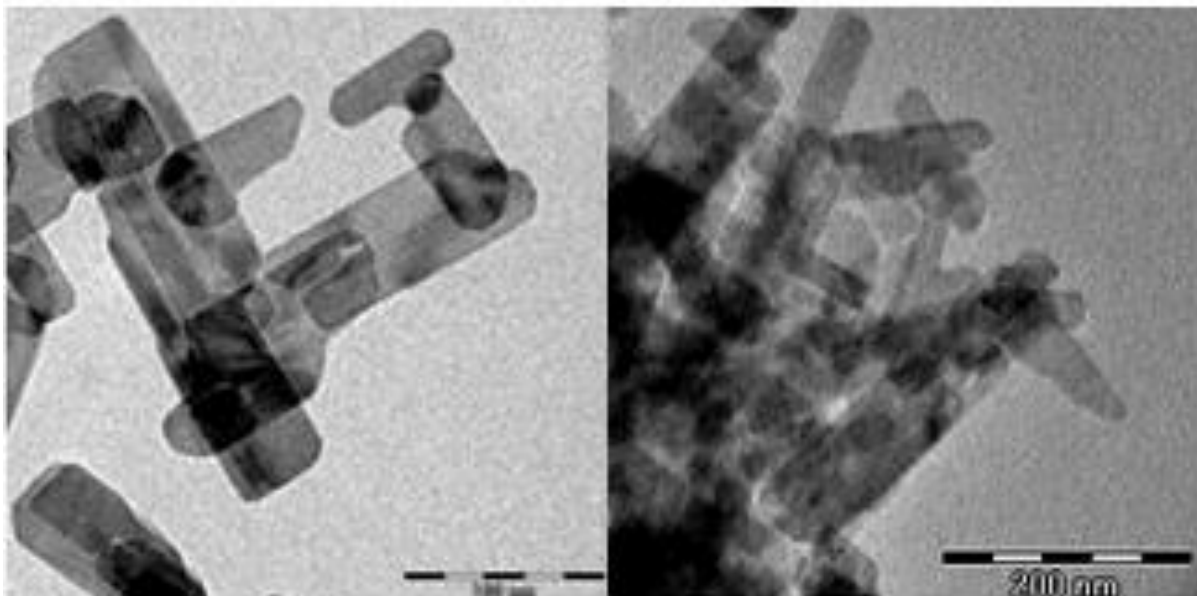


Figure 4.13a TEM images of undoped CdWO₄

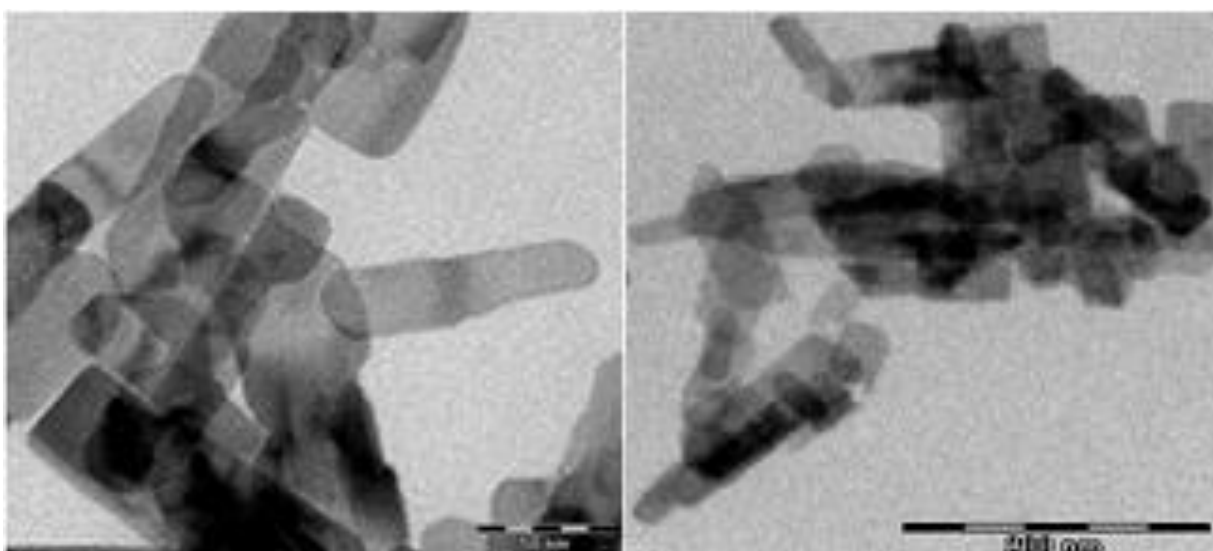


Figure 4.13b TEM images of cerium doped CdWO₄

Figures 4.13a and 4.13b display TEM photographs (at different magnifications) of undoped and cerium-doped samples of the CdWO_4 prepared at 95°C for 12 h hydrothermal conditions. These images show that the formations of nanorods of CdWO_4 are proper, the boundaries are distinct and the rod surface appears quite smooth. It is clear that these CdWO_4 nanorods self-assembled into bundle-like structures. The length of the nanorod is approximately 70-150 nm and the width is about 50nm in can be seen from figure 4a. From figure 4b, it is concluded that doping of Cerium does not affect morphology of cadmium tungstate in terms of its shape and size.

References

1. C. Feldmann, T. Justel, C. R. Ronda, and P. J. Schmidt, *Advanced Functional Materials*. 13, 7,511–516, 2003.
2. A. S. Edelstein and R. C. Cammarata, .Taylor & Francis, London, UK, 1998.
3. Blasee,G. and Grabmaier,B.C. *Luminescent Materials*. Springer-Verlag, Berlin, 1994.
4. S.J. Chen, J.H. Zhou, X.T. Chen, J. Li, L.-H. Li, J.-M. Hong, Z.L. Xue, X.-Z. You, *Chem. Phys. Lett.* 375, 185, 2003.
5. S. Kwan, F. Kim, J. Akana, *Chem. Commun.* 447,2001.
6. B. Liu, S.-H. Yu, F. Zhang, L.J. Li, Q. Zhang, L. Ren, K. Jiang, *J. Phys. Chem. B* 108, 2788, 2004.
7. X.L. Hu, Y. Zhu, *J. Langmuir* 20, 1521,2004.
8. J.T. Klopogge, M.L. Weier, L.V. Duong, R.L. Frost, *Mater. Chem. Phys.* 88, 438, 2004.
9. S.H. Yu, B. Liu, M.S. Mo, J.H. Huang, X.M. Liu, Y.T. Qian, *Adv. Funct. Mater.* 13,639,2003.
10. V. Pankratov, L. Grigorjeva, D. Millers, S. Chernov S, A. Voloshinovskii, *J. Lumin.* 94,427, 2001.
11. Shifan Cheng, Moraga, Yi_Qun Li Walnut Creek; Patent N0: US 7,279,120 B2, Oct. 9, 2007.
12. Yen W M 2005 *Phys. Solid State*, 47, 1393-99, 2005.
13. M. You, J. Xu, Z.Zhang, Y.Zhou ,*Ceramics International* 40,16189–16194,2014.

14. D.K. Chatterjee, A.J. Rufaihah, Y. Zhang, *Biomaterials*, 29, 937, 2008.
15. F. Chen, P. Huang, Y.J. Zhu, J. Wu, C.L. Zhang, D.X. Cui, *Biomaterials*, 32 9031 2011.
16. N.S. White, R.J. Errington, *Adv. Drug Deliver. Rev.*, 57, 17, 2005.
17. J.W. Stouwdam, Ph.D. Thesis, Faculty of Science and Technology, University of Twente, Enschede, The Netherlands, 2003.
18. M.H.V. Werts, *Sci. Prog.*, 88,101, 2005.
19. SanoujamDhirenMeetei, Ph.D. Thesis, Department of Physics, Manipur University,Manipur, India,2014.
20. J GarcíaSolé, L E Bausá and D Jaque, ‘An introduction to the optical spectroscopy of inorganic solids’. John Wiley & Sons, Ltd. New Delhi, India. 283,2005.
21. Lyjo K. Josep, Ph.D Thesis, International School of Photonics,Cochin University of Science & Technology , Feb,2011.
22. D.Tawde, Ph.D. Thesis, Department of Physics, The M S University of Baroda, Gujarat, India,2013.
23. G. Blasse, B.C. Grabmaier, *Luminescent Materials*, Springer, Berlin; London, 1994.
24. <http://www.britannica.com/EBchecked/topic/196533/europium-Eu>.
25. C. Ronda, *Luminescence: From Theory to Applications*, Wiley-VCH, Weinheim, Germany, 2008.
26. G.L. Huang, Y.F.Zhu, *J.Phys.Chem.C.*, 111, 11952–11958,2007.
27. C.T. Sun, D.F.Xue, *Mater.Res.Innovations*17, 27–31, 2013.
28. K.Y. Li,J. J.Shao, D.F.Xue, *Mater. Res.Innovations*17, 218–223, 2013.

29. C.T. Sun, D.F.Xue, Cryst. Eng. Comm16, 2129–2135, 2014.
30. M. Anicete-Santos, E. Orhan, M. A. M. A. de Maurera, L. G.P. Simões, A. G. Souza, P. S. Pizani, E. R. Leite, J. A. Varela, J. Andre´s, A. Beltra´n, and E. Longo, Phys. Rev. B. 75, 165105, 2007.
31. M. Nikl, V. V. Laguta, and A. Vedda, Phys. Status Solidi B.245, 1701, 2008.
32. M. V. Korzhik, Zh. Prikl. Spektrosk. 61, 83, 1994.
33. M. Itoh, D. L. Alov, and M. Fujita, J. Lumin. 87, 1243, 2000.
34. D. L. Alov and S. I. Rybchenco, Mater. Sci. Forum. 239, 279, 1997.
35. M.Nikl, presented at the CCC meeting, May 1995, CERN, W. Van Loo, Phys. Stat. Sol. a. 27,565,1979.
36. J.A. Groenink and G. Blasse , J. Sol. Stat. Chem. 32,1980.
37. P. Lecoq, I. Dafinei, E. Auffray, M. Schneegans, V. Korzhik, O.V. Missevitch, V.B. Pavlenko, A.A. Fedorov, A.N.Annenkov, V.L. Kostylev, Nucl. Instrum. Meth.A 365, 291,1995.
38. D.Tawde,M.Srinivas and K.V.R.Murthy, Phys. Status Solidi A. 208, 4, 803-807,2011.
39. Chai Chunlin, Yang Shaoyan, Liu Zhikai, Liao Meiyong, Chen Nuofu, Wang Zhanguo, Chinese Science Bulletin. 46,24,2046-2048, 2001.
40. Y. Huang, K.H. Jang K, K. Jang, H.J. Seo, J. Lumin. 122-123, 47,2007.
41. K. Polak, M. Niki, K. Nitsch, M. Kobayashi, M. Ishii, Y. Usuki and J. Jarolimerk, J. Lumin., 781,1997.
42. O.V. Rzhetskaya, D.A. Spasskii, V.N. Kolobanov, V.V. Mikhailin, L.L. Nagornaya,I.A. Tupitsina, B.I. Zadneprovskii, Opt. Spectrosc. 104,2008.

43. Y.A. Hizhnyi, S.G. Nedilko and T.N. Nikolaenko, Nucl. Instrum. Methods Phys. Res. A, 537, 2005.
44. Y. C. Kong, D.P.Yu, B. Zhang, W. Fang and S. Q. Feng, Appl. Phys. Lett. 78, 2001.
45. R. Chen, G.Z. Xing, J. Gao, Z. Zhang, T. Wu and H.D. Sun. Appl. Phys Lett. 95, 2009.
46. F. Zhang, B. Liu, J. Alloys Compd. 542, 276–279, 2012.
47. T.T. Dong, Z.H. Li, Z.X. Ding, L. Wu, X.X. Wang, X.Z. Fu, Mater. Res. Bull. 7, 1694, 2008.
48. B. Julian, J. Planelles, E. Cordoncillo, P. Escribano, P. Aschehoug, C. Sanchez, B. Viana, F. Pelle, J. Mater. Chem. 16, 4612, 2006.
49. M. Thomas, P.P. Rao, M. Deepa, M. Chandran, P. Koshy, J. Solid State Chem. 182, 203–207, 2009.
50. X. Mateos, R. Sole', Jna. Gavalda', M. Aguilo', J. Massons, F. Di'az, Optical Materials 28, 423–43, 2006.
51. J. T. Seo, U. H. H'ommerich, A. J. Steckl, B. R. Birkhahn and J. M. Zavada Journal of the Korean Physical Society, 49(3), 943-946, 2006.
52. Hong-tao Sun, Lei Wen, Zhong-chao Duan, Li-li Hu, Jun-jie Zhang and Zhong-hong Jiang, Journal of Alloys and Compounds, 2005
53. Guanqi Chai, Guoping Dong, Jianrong Qiu, Qinyuan Zhang & Zhongmin Yang, Nature – Scientific reports, DOI: 10.1038/srep01598, 2013.
54. X. Mateos, R. Sole, Jna. Gavalda, M. Aguilo, F. Diaz, J. Massons, Journal of Luminescence 115, 131–137, 2005.

55. M.L.DosSantos, R.C.Lima, C.S.Riccardi, R.L.tranquilin, P.R.Bueno, J.A.Varela, E.Longo *Material Letters* 62, 4509-4511, 2008.
56. Zawadzki M, *J Alloys Compd.*451, 347-351, 2008.